Solid State Ionics 276 (2015) 1–8

Contents lists available at ScienceDirect

Solid State Ionics

journal homepage: www.elsevier.com/locate/ssi

Study of ion diffusion in oxidation films grown on a model Fe–15%Cr alloy

Antônio Claret Soares Sabioni [a,*], João Nepomuceno V. Souza [a], Vincent Ji [b], François Jomard [c], Vicente Braz Trindade [d], Jussara F. Carneiro [a]

[a] Departamento de Física, Universidade Federal de Ouro Preto, 35400-000 Ouro Preto, MG, Brazil
[b] ICMMO/SP2M, Université Paris-Sud, 91405 Orsay Cedex, France
[c] CNRS, Université de Versailles-Saint Quentin, France
[d] Departamento de Metalurgia e Materiais, UFOP, Ouro Preto, Brazil

ARTICLE INFO

Article history:
Received 8 December 2014
Received in revised form 6 March 2015
Accepted 18 March 2015
Available online 8 April 2015

Keywords:
Fe–15%Cr alloy
Oxidation
Chromia
Oxygen diffusion
Chromium diffusion
Iron diffusion

ABSTRACT

Chromium, oxygen and iron ion diffusivities were determined in thermally grown natural chromia layer on a model Fe–15 wt.%Cr alloy in the temperature range from 750 °C to 900 °C, in air atmosphere. The stable isotopes ^{18}O, ^{54}Cr and ^{57}Fe were used as oxygen, chromium and iron tracers, respectively, and the diffusion profiles were established by secondary ion mass spectrometry (SIMS). Oxygen bulk, effective and grain boundary diffusivities are lower than the corresponding chromium or iron diffusivities, while the iron diffusivities are greater than the chromium ones. Grain boundary is a fast path for chromium, iron and oxygen ion diffusions in natural chromia layer grown on the Fe–15%Cr alloy. Therefore, the oxidation rate of the Fe–Cr alloy is mainly controlled by grain boundary ion diffusion. The values of the calculated parabolic oxidation constant, according to Wagner's theory, are close to the experimental ones, assuming that chromium and oxygen ion diffusions in chromia grown on the Fe–15%Cr alloy occur in an extrinsic regime. Moreover, chromium ion diffusion plays the main role on the oxidation of the Fe–15%Cr being sufficiently large to maintain the oxidation rate of the alloy.

1. Introduction

The resistance of Fe–Cr based alloys against high temperature oxidation is ensured by the formation of protective chromia layers [1–3]. The growth kinetics of these protective layers follow a parabolic law, which means that the growth rate of the oxide layer is controlled by inward oxygen diffusion from atmosphere or by cation outward diffusion from the metallic substrate or by both cation diffusion and oxygen diffusion [4]. Therefore, it is essential to have knowledge of ion diffusion in these oxide layers to understand the oxidation mechanism and for modeling the high temperature oxidation behavior of such alloys. Direct measurement of ion diffusivities in chromia grown on Fe–Cr based alloys is limited to the studies of Lobnig et al. [5], Horita et al. [6] and Sabioni et al. [7–10]. Lobnig et al. [5] determined cation diffusivities in natural oxide film growth on the alloys Fe–20Cr and Fe–20Cr–12Ni, at 900 °C, while Horita et al. [6] measured the oxygen diffusivity in oxide film grown on the Fe–22 wt.%Cr alloy, at 800 °C. Recently, Sabioni et al. [7–10] studied the oxygen and chromium ion diffusions in oxide layers grown on the AISI 304 austenitic stainless steel (18 wt.%Cr) and on the AISI 439 ferritic stainless steel (17 wt.%Cr), between 750 and 900 °C, in air, and the role of the chromium and oxygen diffusivities on the oxidation of these steels was established.

The present study deals with the study of ion diffusion in oxide films grown on a model Fe–15 wt.%Cr alloy of high purity. The aim is to determine the oxygen, chromium and iron self-diffusion coefficients in the natural oxide film grown on the alloy Fe–15%Cr and, then, to verify the role of these diffusivities on the growth rate of the film.

Oxygen diffusion experiments were performed by means of the isotopic exchange method using the stable isotope ^{18}O as an oxygen tracer [7,9]. Cation (chromium and iron) diffusivities were also studied in the oxide films using the stable isotopes ^{54}Cr and ^{57}Fe as chromium and iron tracers, respectively. These tracers were deposited on the oxidized surface of the alloy followed by the diffusion annealing. The ^{54}Cr, ^{57}Fe and ^{18}O depth profiling was performed by secondary ion mass spectrometry (SIMS). Effective, bulk and grain boundary diffusivities were determined for the tracers in oxide films grown on Fe–15%Cr, from 750 to 900 °C, under oxygen partial pressure of 2.1×10^4 Pa, in synthetic air ($79\%N_2 + 21\%O_2$).

These diffusion data are discussed and compared to the data available in the literature for ion diffusion in oxide films grown on Fe–Cr based alloys.

The high temperature oxidation behavior of the same model Fe–15%Cr alloy used in this study was previously investigated by the authors in the temperature range of 700 °C to 850 °C, in air, and it was found that the oxidation kinetics of this alloy follows a parabolic law [11]. In order to discuss the role of the ion diffusivities on the oxidation of the Fe–15%Cr alloy, the experimental parabolic oxidation constant

* Corresponding author. Tel.: +55 3135591689; fax: +55 3135591660.
E-mail address: claret.sabioni@pq.cnpq.br (A.C.S. Sabioni).

http://dx.doi.org/10.1016/j.ssi.2015.03.027
0167-2738/

was compared to the calculated, according to Wagner's theory, using the chromium and oxygen diffusivities determined in the present study.

2. Experimental procedure

2.1. Materials and preparation of the diffusion specimens

The model Fe–15 wt.%Cr alloy of 99.96% purity was manufactured at Max-Planck Institut für Eisenforschung (Germany). A cylinder bar with 10 mm in diameter was prepared by argon melting process. The average grain size of the alloy was 310 μm. The impurity content (wt.%) in the alloy is as follows: Mn(0.0007), Mg(0.0012), Si(0.0012), P(0.0012), N(0.0019), C(0.011), O(0.0025) and S(0.021). The diffusion specimens, with the dimensions of 4 mm × 4 mm × 2 mm, were cut from the same ingot used to supply the samples for oxidation experiments of this alloy described in a previous work [11].

The larger surfaces of the Fe–15%Cr alloy samples were polished in an automatic grinder/polisher Phoenix 4000/Buehler. The diffusion specimens were initially ground with 1000 and 1200 grit SiC papers, and finally polished with diamond suspensions of 3 and 1 μm respectively. Final cleaning was performed in an ultrasonic acetone bath.

In order to grow the natural oxide films on the alloy for the diffusion experiments, the samples were oxidized at 750, 800, 850 and 900 °C, in synthetic air, for times of 120, 96, 42 and 22 h, respectively. The thicknesses of the chromia films determined from SIMS analyses varied between 0.4 μm, at 750 °C, and 1.0 μm at 900 °C.

Fig. 1a shows the microstructure of the non-oxidized surface of the Fe–15%Cr alloy after chemical etching by Vilella's reagent. Fig. 1b shows the microstructure of the oxidized surface after oxidation at 850 °C, for 42 h, in synthetic air. The average grain size of the oxide films used in the diffusion experiments was submicrometric, varying from 0.4 μm, at 750 °C, to 0.7 μm at 900 °C. For all the conditions used for the oxidation experiments of the Fe–15%Cr, SEM analyses showed that the thermally grown natural oxide films were continuous and adherent to the metallic substrate. Secondary ion mass spectrometry (SIMS) analyses through the oxide film showed chromium as the major element and the presence of some iron whose concentration increases toward the alloy/oxide interface. Analyses by grazing X-ray diffraction (XRD) showed chromia as the only component of the oxide film. Taking into account that hematite and chromia have the corundum structure and form a continuous solid solution in the entire concentration range [12], the iron detected by SIMS is dissolved in the Cr_2O_3 film.

2.2. Chromium and iron diffusion experiments

For the chromium diffusion experiments, the stable isotope ^{54}Cr was used as a chromium tracer. A thin film of ^{54}Cr was deposited on the natural oxide film grown on the Fe–15%Cr alloy by electron-beam evaporation, under ultrahigh vacuum of 2.0×10^{-9} mbar, using an Oxford Applied Research EGCO4 mini evaporator. The deposition rate was 0.2 nm/min and the thickness of the ^{54}Cr layer was about 10 nm as determined by means of a quartz oscillator. Then, the ^{54}Cr diffusion annealing tests were performed from 750 to 900 °C, in flowing synthetic air, using a tubular furnace.

For the iron diffusion experiments, the stable isotope ^{57}Fe was used as an iron tracer. A thin film of ^{57}Fe was deposited on the oxidized surface of the alloy by using the same conditions of the chromium deposition. Then, the iron diffusion annealing tests were performed from 750 to 850 °C, in air atmosphere.

Both isotopes ^{54}Cr and ^{57}Fe were supplied by Euriso-top, Saint-Aubin, France, and their isotopic compositions as well as the impurity contents are given in Tables 1 and 2, respectively.

2.3. Oxygen diffusion experiments

After preparing the oxide film on the Fe–15%Cr alloy, in synthetic air, as described in Section 2.1, the oxygen ion diffusion experiments were performed by means of the isotopic exchange method using the stable isotope ^{18}O as an oxygen tracer [7,9]. The diffusion studies were performed from 750 to 900 °C, in a static atmosphere of argon + 21%$^{18}O_2$ mixture ($P_{O_2} = 2.1 \times 10^4$ Pa). The $^{18}O_2$ gas used in the experiments was supplied by ISOTEC (Sigma-Aldrich)/U.S.A.

2.4. Tracer depth profiling by secondary ion mass spectrometry (SIMS)

After the diffusion annealing, the depth diffusion profiles of the tracers ^{54}Cr, ^{57}Fe or ^{18}O were established by secondary ion mass spectrometry (SIMS) using an Apparatus CAMECA IMS3/4F (magnetic sector dynamic SIMS). A 10 keV O^+ primary ion source was used for analyzing chromium or iron isotopes, while for the oxygen diffusion profiles a 10 keV Cs^+ primary ion source was used. The current intensity of the primary ion beam was about 20 nA, and the incidence angle was of 27° with respect to the normal to the surface of the sample. The scanned area by the primary ion beam, during the SIMS analyses, was 200 μm × 200 μm, and the intensities of the negative ionic signals of the isotopes I($^{50}Cr^-$), I($^{52}Cr^-$), I($^{53}Cr^-$), I($^{54}Cr^-$), for chromium; I($^{54}Fe^-$), I($^{56}Fe^-$), I($^{57}Fe^-$), I($^{58}Fe^-$), for iron; and I($^{16}O^-$) and I($^{18}O^-$), for oxygen, were collected as a function of the sputtering time from a zone of 62 μm in diameter centered on the scanned area. The typical sputtering rate of the sample surface was about 0.5 nm/s. For each tracer, the diffusion profiles, as a function of the sputtering time, were determined from the intensities of the signals of the negative ions using procedures already described in previous works [13–15].

The conversion of the concentrations C(^{57}Fe), C(^{54}Cr) or C(^{18}O) versus sputtering time into C(^{54}Cr), C(^{57}Fe) or C(^{18}O) versus penetration depth was performed by measuring the depth of the crater produced

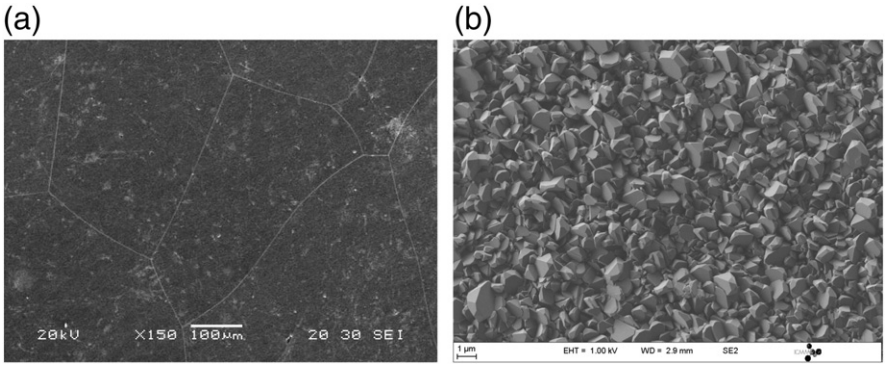

Fig. 1. SEM analyses of the surface of the Fe–15Cr% alloy before and after the oxidation. (a) Non-oxidized surface of the alloy after chemical etching by Vilella's reagent; (b) microstructure of the oxidized surface, after 42 h at 850 °C, in air.

Table 1
Chemical analysis of natural and enriched chromium isotope.

Isotopic composition of natural chromium				
Isotope	50	52	53	54
%	4.35	83.79	9.50	2.36

Isotopic composition of chromium used as a tracer				
Isotope	50	52	53	54
%	<0.01	<0.05	0.20	99.8

Metallic impurities of the chromium used as a tracer												
Element	Al	Ca	Co	Cu	Fe	Ge	Mg	Mn	Na	Ni	Sc	Si
ppm	144	144	<50	14	90	65	14	65	3.5	<50	<50	107

by the sputtering on the surface during the SIMS analysis, using a Talystep profilometer.

Fig. 2a shows an example of a SIMS analysis of the chromia grown on the oxide film grown on the Fe–15%Cr alloy, after iron diffusion at 750 °C. In the SIMS analysis of Fig. 2a the intensities of the ionic signal of the isotopes $^{54}Fe^-$, $^{56}Fe^-$, $^{57}Fe^-$, $^{58}Fe^-$, $^{18}O^-$, and $52Cr^-$ are displayed. For all the studied cases, the ionic signals of the tracers were taken only inside the chromia rich region of the film, as that delineated by the dot line in the plot of Fig. 2a. Fig. 2b shows the plot of ^{57}Fe concentration versus penetration depth determined from the SIMS analysis of Fig. 2a.

2.5. Determination of the ion diffusion coefficients

For the experimental conditions used in this study, the diffusion profiles correspond to the B-type intergranular diffusion [16], whose depth profiles present two different regions as shown in Fig. 2b. The first part of the diffusion profile, near the surface and with high concentration gradient, should correspond to the bulk diffusion, whereas the second part, in the tail of the curve, with low concentration gradient, corresponds to the grain boundary diffusion.

Due to the submicrometric grain size of the microstructures of the oxide layers grown on Fe–15%Cr, there are a very high number of grains in the region analyzed by SIMS. For such case, as described elsewhere [17,18], it has been usually assumed that the first part of the diffusion profiles corresponds to an effective diffusion instead of bulk diffusion. This effective diffusion is a combination of bulk diffusion plus grain boundary diffusion. The effective diffusion coefficient (D_{eff}) may be calculated by means of Hart's equation as follows [19]:

$$D_{eff} = fD_{gb} + (1-f)D_b \quad (1)$$

where D_b is the bulk diffusion coefficient, D_{gb} is the grain boundary diffusion coefficient and f is the fraction of the atomic sites associated to the grain-boundaries, that may be calculated by means of the usual expression $f = 3\delta / \Phi$, where Φ is the grain size of the microstructures and δ is the grain boundary width. The value of δ is generally assumed to be equal to 1 nm [20].

For B-type intergranular diffusion, the product δD_{gb} may be calculated by means of Le Claire's equation given by [21]:

$$\delta D_{gb} = 1.32\left(\frac{D_b}{t}\right)^{1/2}\left(-\frac{d\ln C(x)}{dx^{6/5}}\right)^{-5/3} \quad (2)$$

where $C(x)$ is the concentration of the tracer at the depth x, and the gradient $d\ln C(x)/dx^{6/5}$ is determined from the tail of the diffusion profile in the plots of $\ln C(x) = f(x^{6/5})$.

In this study, the values of D_b and D_{gb} were calculated by resolving the system formed by Eqs. (1) and (2), using the values of D_{eff} and $d\ln C(x)/dx^{6/5}$ previously determined.

3. Results and discussions

3.1. Ion diffusion in oxide films grown on the Fe–15%Cr alloy and comparison with available data in literature

3.1.1. Oxygen ion diffusion

Fig. 3a shows the oxygen diffusion profile in chromia grown on the Fe–15%Cr alloy, after diffusion at 800 °C, and Fig. 3b shows the plot of $\ln C(x)$ versus $x^{6/5}$ corresponding to the diffusion profile of Fig. 3a. The oxygen effective diffusion coefficient (D_{eff}) was determined from the diffusion profiles in the region near the surface by using a solution of Fick's second law for diffusion in a semi-infinite medium from a constant surface concentration given by [22]:

$$\frac{C(x)-C_s}{C_o-C_s} = \mathrm{erf}\left(\frac{x}{2\sqrt{D_{eff}t}}\right) \quad (3)$$

where C_s is the constant concentration of the tracer at the surface, $C(x)$ is the tracer concentration at the depth x, C_o is the natural abundance of ^{18}O (0.20%), t is the diffusion annealing time, and erf is the error function. The effective diffusion coefficient was determined by fitting Eq. (3) to the first part of the oxygen diffusion profile by nonlinear regression.

The results obtained for the ^{18}O effective, bulk and grain boundary diffusivities, as well as the experimental conditions are given in Table 3.

Oxygen diffusivities have been measured in synthetic chromia (single crystalline and hot-pressed samples), but only at higher temperatures (≥1100 °C) [14,23–25], which prevents direct comparison. In spite of its importance for understanding the oxidation phenomenon, data about oxygen diffusion in thermally grown oxides on Fe–Cr based alloys have been determined only recently [6,7,9]. It is interesting to gather such available data for different Fe–Cr based alloys and compare them with the present results as shown in Fig. 4.

In previous studies, Sabioni et al. [7,9] measured the oxygen diffusivities in oxides films grown on AISI 304 austenitic stainless steel and on AISI 439 ferritic stainless steel in the temperature range of 750–900 °C, in Ar + 21%$^{18}O_2$ atmosphere. It was demonstrated that the oxygen diffusion is more important than the chromium diffusion for the oxidation of AISI 304 or AISI 439 stainless steels.

Another data was determined by Horita et al. [6] in oxide films grown on a Fe–22 wt.%Cr alloy at 800 °C, under an oxygen partial pressure of 10^4 Pa. The data of Horita et al. [6] were determined only from the initial part of the diffusion profiles, at 800 °C, and should correspond to an effective or bulk diffusion coefficient. Their results were found to be too large, even greater than the set of values of intergranular diffusivities displayed in Fig. 4. Horita et al. have not found an explanation for this high oxygen diffusivity ($3.1–5.4 \times 10^{-12}$ cm^2/s), too large to be related to the oxidation constant of their alloy (~10^{-14} cm^2/s).

The oxygen diffusivities in oxide films grown on the Fe–15%Cr alloy are lower than in the oxide layers grown on the AISI 304 and AISI 439

Table 2
Chemical analysis of natural and enriched iron isotope.

Isotopic composition of natural iron				
Isotope	54	56	57	58
%	5.8	91.72	2.2	0.28

Isotopic composition of iron used as a tracer				
Isotope	54	56	57	58
%	0.01	2.7	96.59	1.59

Metallic impurities of the iron used as a tracer								
Element	Al	C	Cr	Cu	Mg	Ni	Si	Zn
ppm	<100	730	<100	<100	<100	<100	<100	<100

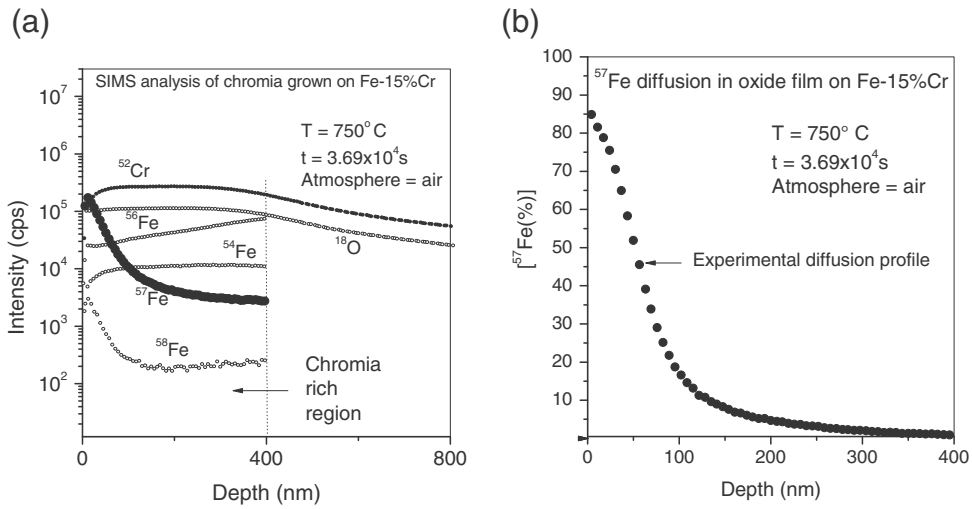

Fig. 2. (a) SIMS analysis of the chromia grown on Fe–15%Cr after ^{57}Fe diffusion at 750 °C, and (b) the corresponding depth diffusion profile of the ^{57}Fe.

steels, in the same experimental conditions. Probably, the metallic impurities in the natural oxide films grown on these stainless steels affect the point defect structure of the oxide and, consequently, the oxygen diffusivities. Under the practical point of view, the interpretation of the role of impurities on the ion oxygen diffusion in thermally grown oxide films on stainless steels is complicated, because the concentration of the metallic impurities in the chromia film continuously varies through the film.

3.1.2. Chromium ion diffusion

Fig. 5a shows the chromium diffusion profile at 900 °C and the Fig. 5b shows the corresponding plot of $\ln C = f(x^{6/5})$.

The effective diffusion coefficient of the chromium was determined from the first part of the diffusion profile by using a solution of Fick's second law for diffusion in a semi-infinite medium from a superficial thin film given by [22]:

$$C(x) = C_o \exp\left(-x^2/4tD_{eff}\right) \quad (4)$$

where $C(x)$ is the concentration at the depth x, C_o is a constant, t is the diffusion annealing time and D_{eff} is the effective diffusion coefficient.

The chromium bulk and grain boundary diffusivities were determined in oxide films grown on the Fe–15%Cr alloy by using Eqs. (1) and (2), as previously described in Section 2.5. The experimental conditions and the results obtained for the chromium diffusivities are listed in Table 4.

In the case of chromium diffusion, there are several earlier studies performed on single crystalline and hot-pressed chromia, but at higher temperatures (1050–1570 °C), which does not enable a direct comparison with the present data. These data are reviewed elsewhere [17,18,26,27].

Studies of chromium diffusion in oxide films grown on Fe–Cr based alloys are limited to the studies of Lobnig et al. [5] and Sabioni et al. [8,10]. These data are compared in Fig. 6 with the results of the present study. Lobnig et al. measured the chromium bulk and grain boundary diffusion coefficients in oxide films grown on the alloys Fe–20Cr–Ni and Fe–20Cr, at 900 °C [5].

The results of Lobnig et al. were determined in the first part of the diffusion profile as being bulk diffusivity, but they are comparable to the effective diffusivities of Cr in the oxide layers grown on the other Fe–Cr based alloys. On the other hand, the grain boundary diffusion coefficients determined by Lobnig et al. are too high ($>10^{-10}$ cm^2/s) and they are not represented in Fig. 6.

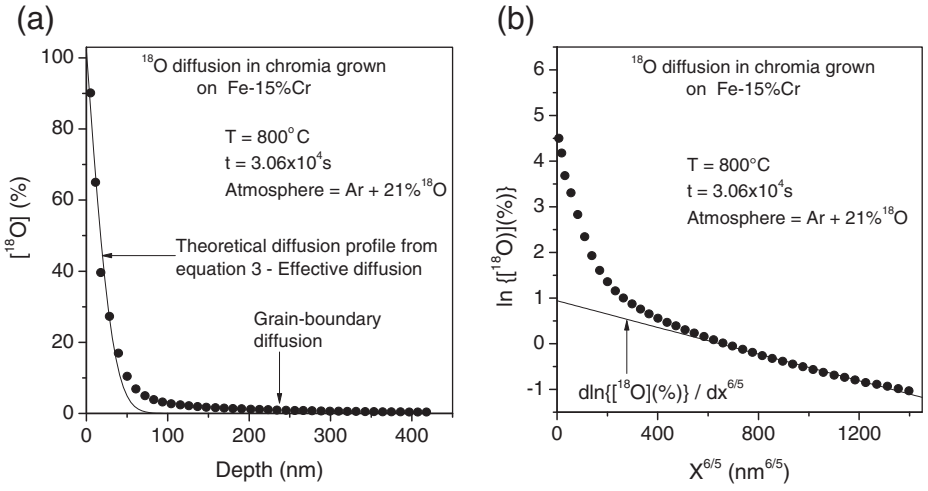

Fig. 3. (a) ^{18}O depth profile in chromia grown on the Fe–15%Cr alloy after diffusion at 800 °C, and (b) the corresponding plot of $\ln C = f(x^{6/5})$.

Table 3
^{18}O diffusion coefficients determined in oxide films grown on the Fe–15%Cr alloy.

T (°C)	t (s)	D_{eff} (cm^2/s)	D_b (cm^2/s)	D_{gb} (cm^2/s)	D_{gb}/D_b
750	4.23×10^4	3.4×10^{-17}	5.7×10^{-20}	4.8×10^{-15}	8.4×10^4
800	3.06×10^4	1.0×10^{-16}	1.8×10^{-19}	1.7×10^{-14}	9.4×10^4
850	2.16×10^4	3.0×10^{-16}	3.0×10^{-19}	5.3×10^{-14}	1.8×10^5
900	7.20×10^3	1.8×10^{-15}	5.2×10^{-18}	4.4×10^{-13}	8.5×10^4

Recently, Sabioni et al. determined the chromium effective, bulk and grain boundary diffusivities in oxide films grown on the AISI 304 austenitic stainless steel, between 750 and 850 °C [8], and on AISI 439 ferritic stainless steels, between 750 and 900 °C [10], in air, using the same methodology as used in the present study. As shown in Fig. 6, the grain boundary is a fast path for chromium diffusion in oxide layers grown on the model Fe–15%Cr alloys and on the AISI 304 and AISI 439 steels. Besides, the chromium grain boundary diffusivities in oxide films grown on the model Fe–15%Cr alloy and on the AISI 304 and AISI 439 steels vary within a narrow range of values of less than half order of magnitude.

3.1.3. Iron ion diffusion

The iron diffusion in chromia grown on the Fe–15%Cr alloy was studied from 750 to 850 °C, in air.

The iron diffusivities in Cr_2O_3 grown on the Fe–15%Cr alloy were determined with the same mathematical procedure used for chromium diffusivities. The fitting of Eq. (4) to the ^{57}Fe diffusion profile to determine the effective iron diffusivity, after diffusion at 750 °C, is shown in Fig. 7a. The plot of $\ln C(x) = f(x^{6/5})$ corresponding to the iron diffusion profile of Fig. 7a is shown in Fig. 7b.

For the experiment at 850 °C, the tail of the diffusion profile was not long enough inside the chromia rich region to allow the determination of the gradient $d\ln C(x)/dx^{6/5}$. The experimental conditions and the results obtained for the iron diffusivities are shown in Table 5.

Data on iron diffusion in thermally grown chromia films is even more limited in the literature. As far as we know, the only study about iron diffusion in chromia grown on Fe–Cr based alloys is that of Lobnig et al. [5] who measured iron diffusivities in Fe–20Cr and Fe–20Cr–12Ni alloys, at 900 °C. Sabioni et al. [15] measured iron diffusivities in synthetic polycrystalline Cr_2O_3 (hot pressed — HP), between 740 °C and 1100 °C, and in a chromia layer grown on a Ni–30Cr alloy in the temperature range of 720–900 °C, in an atmosphere of Ar + 100 ppm O_2 ($P_{O_2} = 10$ Pa), and at 900 °C in air atmosphere ($P_{O_2} = 2.1 \times 10^4$ Pa). No effect of the oxygen pressure was observed on the iron diffusion. These available data are compared to the present results in Fig. 8.

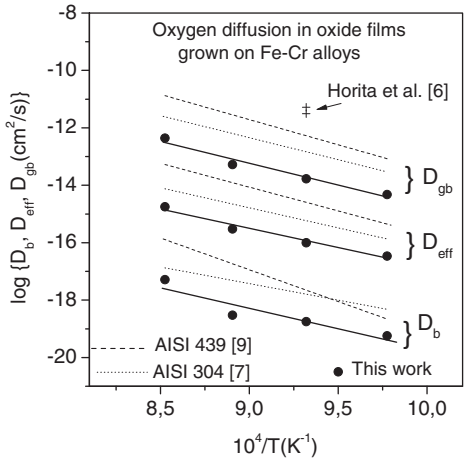

Fig. 4. Comparison of oxygen diffusivities determined in the present studies with literature data for chromia grown on Fe–Cr based alloys.

As for chromium diffusion experiments, Lobnig's data for bulk diffusion are comparable to iron effective diffusivities found on this study. It is worth noting that the iron bulk and grain boundary diffusivities in polycrystalline chromia and the effective and grain boundary diffusion in the chromia film, previously determined [15], are close to the results of the present study. Such as for chromium diffusion, the iron grain boundary diffusion in the oxide layer also appears not to depend on the chromia forming alloys.

3.2. Comparison of the oxygen, chromium and iron diffusivities in natural chromia layers grown on the Fe–15%Cr alloy

The oxygen, chromium and iron diffusivities in the model Fe–15%Cr are compared in the Arrhenius diagram of Fig. 9. This direct comparison of the ion diffusivities in the oxide films grown on the Fe–15%Cr alloy, between 750 and 900 °C, in air atmosphere, leads to the following conclusions: (i) oxygen diffusivities are lower than the chromium or iron diffusivities; (ii) iron diffusivities are greater than the chromium ones; and (iii) grain boundary is a fast path for chromium, iron and oxygen ion diffusions ($D_{gb} \sim 10^4$–$10^5 D_b$) in thermally grown chromia.

As iron diffusivities are greater than chromium or oxygen diffusivities, the chromia film grown on the Fe–15%Cr alloy is not a barrier for the diffusion of iron. Probably, the iron diffusion in the oxide film grown on the Fe–15%Cr alloy is thermodynamically limited by the low oxygen pressure in the metal/oxide interface, which hampers the oxidation of the iron and its incorporation into the oxide [15].

It should be emphasized that the chromium diffusivities greater than oxygen diffusivities in chromia films, as observed in this and other studies [18], should not be considered as a general rule. Contrarily, in the oxidation of AISI 304 and AISI 439 stainless steels [8,10], the oxygen ion diffusivities in oxide films are greater than the chromium diffusivities and play the main role on the oxidation of these steels. Therefore, the relation between chromium and oxygen diffusions in thermally grown oxide films depends on the composition of the chromia forming alloy.

3.3. Role of the chromium and oxygen ion diffusions on the oxidation of the Fe–15%Cr alloy

The high temperature oxidation behavior of model Fe–xCr alloys (x varying from 1.5% to 15 wt.% of Cr) has been studied [11], between 700 and 850 °C, in flowing synthetic air atmosphere, for 48 h. For these experimental conditions, the growth kinetics of chromia on the Fe–15%Cr alloy was found to obey a parabolic law given by $(\Delta M/S)^2 = k_p t + b$, where $\Delta M/S$ is the mass gain per unit surface area, k_p (g^2 cm^{-4} s^{-1}) is the parabolic oxidation constant, t is the oxidation time and b is a constant. The dependence on temperature of the k_p values of this previous study [11] may be described by the following Arrhenius' relationship:

$$k_p\left(g^2/cm^4\ s\right) = 3.4 \times 10^{-5} \exp\left[-\frac{178.6\ kJ/mol}{RT}\right]. \quad (5)$$

The relationship between ion diffusion through the oxide film and the oxidation rate of the Fe–15%Cr alloy may be verified by comparing parabolic oxidation rate constants calculated according to Wagner's theory [4], using the ion diffusivities obtained in the present work, with the available experimental parabolic oxidation constant given by Eq. (5).

The parabolic oxidation constant may be calculated by means of Wagner's theory through the following relationship [4]:

$$k_c\left(cm^2/s\right) = \int_{P_{O_2}^{int}}^{P_{O_2}^{ext}} \left(1.5 D_{Cr}^{eff} + D_O^{eff}\right) d\ln P_{O_2} \quad (6)$$

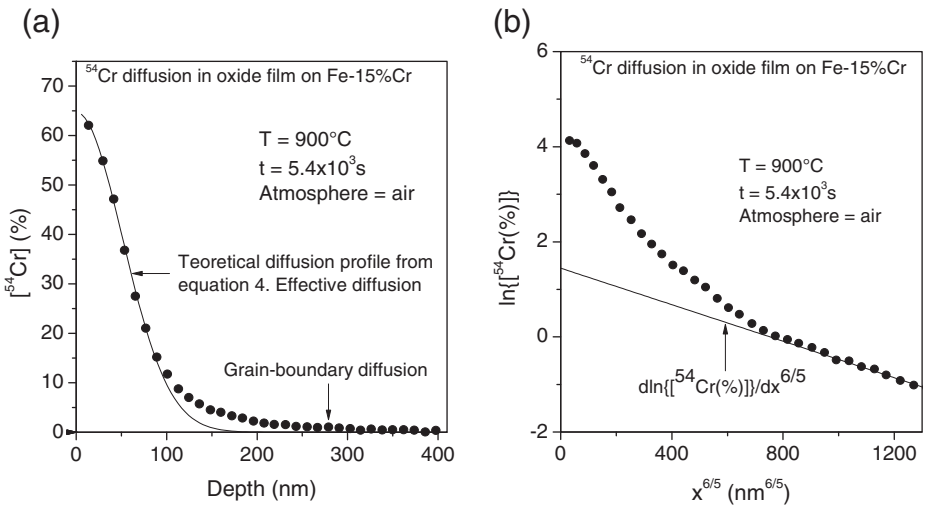

Fig. 5. (a) ^{54}Cr diffusion profile at 900 °C, and (b) the corresponding plot of $\ln C = f(x^{6/5})$.

where k_c is the parabolic oxidation constant, expressed in cm^2/s, $P_{O_2}^{ext}$ is the oxygen pressure at the interface oxide/atmosphere (equal to 2.1×10^4 Pa), $P_{O_2}^{int}$ is the oxygen pressure at the interface metal/oxide (determined from Ellingham's diagram for the equilibrium $4/3Cr + O_2 = 2/3Cr_2O_3$ as 10^{-24} to 8×10^{-18} Pa in the range of 750–900 °C), D_{Cr}^{eff} is the effective chromium diffusion coefficient and D_O^{eff} is the effective oxygen diffusion coefficient.

To calculate k_c by means of Eq. (6), the dependency of ion diffusion with oxygen pressure at a given temperature should be known. In the present moment, there is no data on chromium or oxygen ion diffusion in chromia grown on Fe–15%Cr, or on other Fe–Cr based alloys, or even in synthetic chromia, as a function of the oxygen pressure in the temperature range of the present work.

Due to the lack of data about a possible effect of oxygen pressure on ion diffusion in chromia, the parabolic oxidation constant (k_c) will be estimated by means of Eq. (6), taking into account two different possibilities. Firstly, the ion diffusion will be assumed not to depend on the oxygen pressure, i.e., the ion diffusion takes place in an extrinsic regime. Secondly, it will be assumed that the ion diffusion may depend on the oxygen pressure. Taking into account these two assumptions, the values of k_c given by Eq. (6) should define a range of values within which the experimental oxidation constant should fall.

Thus, if it is assumed that the ion diffusion occurs in an extrinsic regime, Eq. (6) may be rewritten as follows [1]:

$$k_c\left(cm^2/s\right) = \left(1.5D_{Cr}^{eff} + D_O^{eff}\right) \ln \frac{P_{O_2}^{ext}}{P_{O_2}^{int}}. \quad (7)$$

On the other hand, to evaluate a possible effect of ion diffusion dependence on oxygen pressure, the same methodology as used by Tsai et al. [18] was applied to relate oxygen and chromium ion diffusion with the oxidation rate of chromia grown on a Ni–30%Cr alloy, in experimental conditions similar to those of the present study. Considering that ion self-diffusion takes place by means of chromium vacancies (VCr‴) and interstitial oxygen (Oi″), and considering for chromium and oxygen diffusions $D_{Cr}^{eff} = D_{Cr}^{o,eff} \cdot P_{O_2}^{3/16}$ and $D_O^{eff} = D_O^{o,eff} \cdot P_{O_2}^{1/16}$, respectively, being $D^{o,eff}$ the effective ion diffusivity at $P_{O_2} = 1$ atm $\left(= 10^5 Pa\right)$, Tsai et al. established from Eq. (6) the following relationship [18]:

$$k_c\left(cm^2/s\right) = 6D_O^{eff}\left(P_{O_2}^{ext}\right) + 8D_{Cr}^{eff}\left(P_{O_2}^{ext}\right) \quad (8)$$

where $D_O^{eff}\left(P_{O_2}^{ext}\right)$ and $D_{Cr}^{eff}\left(P_{O_2}^{ext}\right)$ are the oxygen and effective chromium diffusivities determined under an oxygen pressure corresponding to that of the interface oxide/atmosphere, which is 2.1×10^4 Pa in our case.

For comparing the calculated and experimental parabolic oxidation constants, the experimental values of k_p ($g^2\ cm^{-4}\ s^{-1}$), given by Eq. (5), were converted into k_c (cm^2/s) by using the expression [1]:

$$k_c\left(cm^2/s\right) = (M_{ox}/3\rho_{ox}M_o)^2 k_p\left(g^2\ cm^{-4}\ s^{-1}\right) \quad (9)$$

where M_o, M_{ox} and ρ_{ox} are the molar mass of oxygen, the molar mass of Cr_2O_3, and the density of Cr_2O_3, respectively.

The parabolic oxidation rate constant was firstly calculated by means of Eq. (7) taking into account the following three cases: considering only oxygen diffusion, $k_c(^{18}O)$; considering only chromium diffusion, $k_c(^{54}Cr)$; and finally the simultaneous effect of the oxygen and chromium diffusion, $k_c(^{18}O + {}^{54}Cr)$, was considered.

Table 4
^{54}Cr diffusivities determined in oxide films grown on the Fe–15%Cr alloy.

T (°C)	t (s)	D_{eff} (cm^2/s)	D_b (cm^2/s)	D_{gb} (cm^2/s)	D_{gb}/D_b
750	3.24×10^4	2.0×10^{-16}	1.7×10^{-19}	2.8×10^{-14}	1.6×10^5
800	2.16×10^4	2.6×10^{-16}	2.2×10^{-18}	4.4×10^{-14}	2.0×10^4
850	1.44×10^4	5.0×10^{-16}	5.8×10^{-18}	8.7×10^{-14}	1.5×10^4
900	5.4×10^3	2.3×10^{-15}	8.0×10^{-17}	5.4×10^{-13}	6.8×10^3

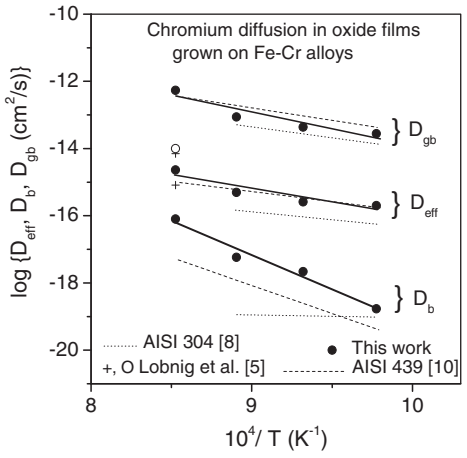

Fig. 6. Comparison of chromium diffusivities determined in the present studies with literature data for chromia grown on Fe–Cr alloys.

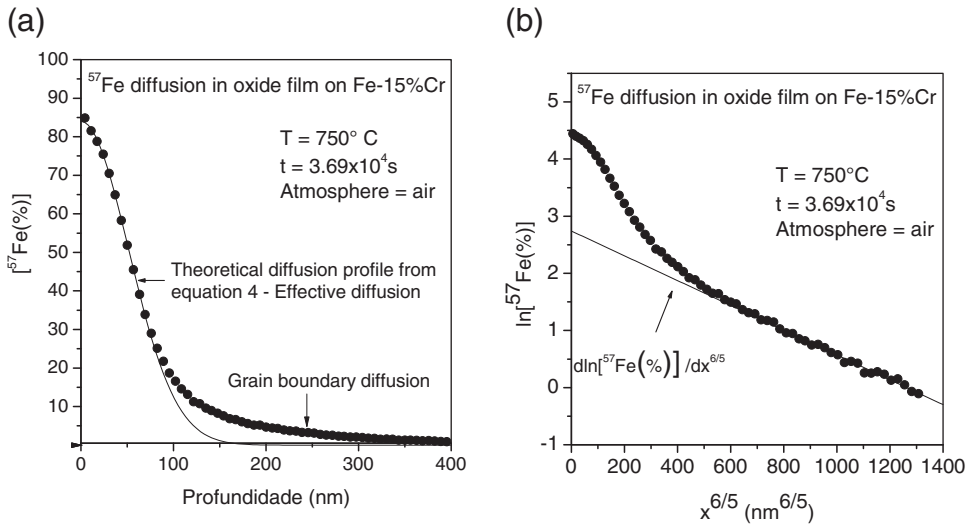

Fig. 7. (a) ^{57}Fe depth profile in chromia grown on the Fe–15%Cr alloy after diffusion at 750 °C, and (b) the corresponding plot of $\ln C = f(x^{6/5})$.

Table 5
^{57}Fe diffusivities determined in oxide films grown on the Fe–15%Cr alloy.

T (°C)	t_d (s)	D_{eff} (cm^2/s)	D_b (cm^2/s)	D_{gb} (cm^2/s)	D_{gb}/D_b
750	3.69×10^4	3.6×10^{-16}	6.9×10^{-18}	4.9×10^{-14}	7.1×10^3
800	2.40×10^4	6.5×10^{-16}	1.0×10^{-17}	1.1×10^{-13}	1.1×10^4
850	2.46×10^4	3.4×10^{-15}			

According to Fig. 10, the values calculated by means of Eq. (7) show that: (i) The oxygen diffusion is not sufficiently large to maintain the oxidation rate of the Fe–15%Cr alloy, (ii) chromium diffusion is enough to maintain the oxidation rate of the alloy in the whole temperature range, in air, and (iii) the simultaneous oxygen and chromium ion diffusions lead to calculated parabolic oxidation rate constants slightly greater than the experimental ones, whereby this difference is smaller than half an order of magnitude. On the other hand, the values of calculated k_c, given by Eq. (8), are smaller than the experimental ones. Thus, according to Fig. 10, the values of the experimental k_c are closer to the values of k_c calculated by means of Eq. (7) that describes reasonably the oxidation rate of the model Fe–15%Cr alloy. This result indicates that the ion diffusion in oxide films grown on the Fe–15%Cr alloy does not depend on the oxygen partial pressure, which will be the subject of further studies.

4. Conclusions

- For the first time, oxygen, chromium and iron ion diffusivities were measured in thermally grown chromia on a Fe–15%Cr alloy in the temperature range of 750–900 °C, in synthetic air.
- Oxygen bulk, effective and grain boundary diffusivities are lower than the corresponding chromium or iron diffusivities.
- Iron diffusivities are greater than the chromium ones. Therefore, a chromia film grown on a Fe–15%Cr alloy is not a physical barrier but a thermodynamic one for the iron diffusion due to the very low oxygen pressure at the metal/oxide interface.
- Grain boundaries are fast paths for chromium, iron and oxygen ion diffusions in chromia grown on a Fe–15%Cr alloy. Therefore, the oxidation rate of the alloy is mainly controlled by grain boundary ion diffusion.
- The values of the experimental parabolic oxidation constant are close to those calculated, using Wagner's theory, assuming that chromium and oxygen ion diffusivities do not depend on oxygen pressure. Moreover, chromium ion diffusion plays the main role on the oxidation of the Fe–15%Cr being sufficiently high to ensure the growth rate of the oxide film.

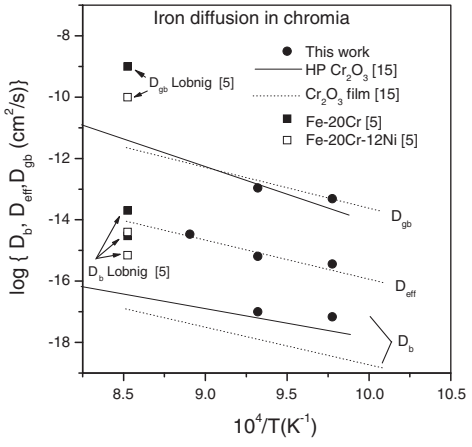

Fig. 8. Comparison of iron diffusivities determined in the present studies with literature data for chromia grown on Fe–Cr or Ni–Cr alloys and in synthetic chromia.

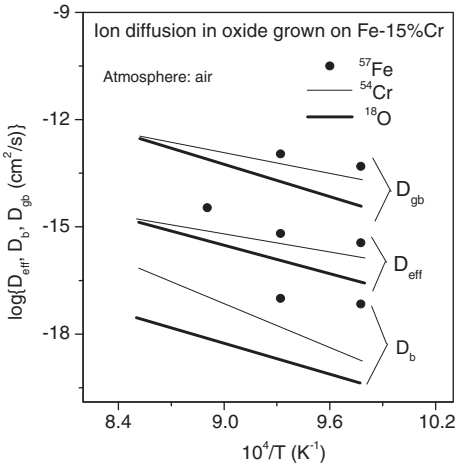

Fig. 9. Comparison of the oxygen, iron and chromium ion diffusivities in chromia grown on Fe–15%Cr.

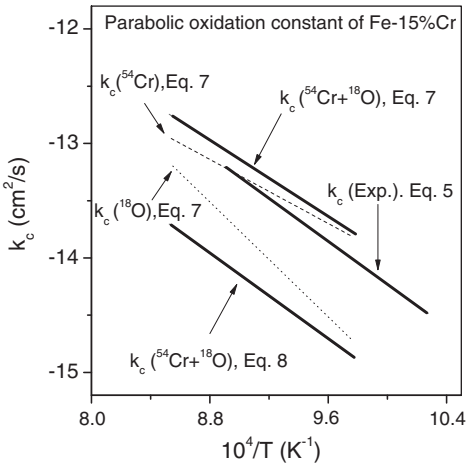

Fig. 10. Comparison of experimental k_c with calculated k_c given by Eqs. (7) and (8).

Acknowledgments

The authors are grateful to FAPEMIG (PPM N° 00171-09) and CNPq (N° 476913/2008-0) Brazilian Agencies, and to CNRS/France (N° 9143RA12) by financial support. The authors also thank Dr. Waldemar Macedo for the preparation of chromium and iron thin films at the Nuclear Technology Development Center (Brazil). The authors would like to pay tribute to Prof. A. M. Huntz for her contribution to the field of oxidation.

References

[1] A.M. Huntz, A. Reckmann, C. Haut, C. Sévérac, M. Herbst, F.C.T. Resende, A.C.S. Sabioni, Mater. Sci. Eng. A 447 (2007) 266–276.
[2] A.S. Khanna (Ed.), ASM International, The Materials Information Society, 2002 (321 pp.).
[3] A.C.S. Sabioni, A.M. Huntz, E.C. Luz, M. Mantel, C. Haut, Mater. Res. 6 (2003) 179–185.
[4] C. Wagner, Atom Movements, ASM Seminar, Cleveland, 1951. 153–173.
[5] R.E. Lobnig, H.P. Schmidt, K. Hennesen, H.J. Grabke, Oxid. Met. 37 (1992) 81–93.
[6] T. Horita, K. Yamaji, Y. Xiong, H. Kishimoto, N. Sakai, H. Yokokawa, Solid State Ionics 175 (1–4) (2004) 157–163.
[7] A.C.S. Sabioni, R.P.B. Ramos, V. Ji, F. Jomard, Defect. Diffus. Forum 323 (2012) 345–352.
[8] A.C.S. Sabioni, P.R.B. Ramos, V. Ji, F. Jomard, W.A.A. Macedo, P. Lana, V.B. Trindade, Oxid. Met. 78 (2012) 211–220.
[9] A.C.S. Sabioni, E.A. Malheiros, V. Ji, F. Jomard, Defect. Diffus. Forum 323 (2012) 339–344.
[10] A.C.S. Sabioni, E.A. Malheiros, V. Ji, F. Jomard, W.A.A. Macedo, P.L. Gastelois, Oxid. Met. 81 (3) (2014) 407–419.
[11] J.F. Carneiro, V.B. Trindade, V. Ji, A.C.S. Sabioni, Congresso Brasileiro de Engenharia e Ciência dos Materiais - CBECiMat, Campos do Jordão, São Paulo, Brasil, 19 2010, pp. 5980–5988.
[12] T. Grygar, P. Bezdicka, J. Dedecek, E. Petrovsky, O. Schneeweis, Ceram.-Silikáty 47 (1) (2003) 32–39.
[13] A.C.S. Sabioni, B. Lesage, A.M. Huntz, J. Pivin, J. Philibert, C. Monty, Philos. Mag. A 66 (1992) 333–350.
[14] A.C.S. Sabioni, A.M. Huntz, F. Millot, C. Monty, Philos. Mag. A 66 (1992) 351–360.
[15] A.C.S. Sabioni, A.M. Huntz, F. Silva, F. Jomard, Mater. Sci. Eng. A Struct. Mater. 392 (2005) 254–261.
[16] L.G. Harrison, Trans. Faraday Soc. 57 (1961) 1191–1199.
[17] S. Chevalier, Defect. Diffus. Forum 405–412 (2009) 289–292.
[18] S.C. Tsai, A.M. Huntz, C. Dolin, Mater. Sci. Eng. A 212 (1996) 6–13.
[19] E.W. Hart, Acta Metall. 5 (1957) 597.
[20] A. Atkinson, R.I. Taylor, Philos. Mag. A 43 (1981) 999–1015.
[21] A.D. Le Claire, Br. J. Appl. Phys. 14 (1963) 351–366.
[22] J. Philibert, Atom Movements, Diffusion and Mass Transport in Solids, Les Editions de Physique, Les Ulis, France, 1991.
[23] A.C.S. Sabioni, A.M. Huntz, F. Millot, C. Monty, Philos. Mag. A 66 (1992) 361–374.
[24] W.C. Hagel, J. Am. Ceram. Soc. 48 (1965) 70–75.
[25] W.E. King, J.H. Park, Conf. Proceedings Materials Research Society Spring, Mtg., Reno, Nevada, vol. 122 1988, pp. 193–198.
[26] P. Kofstad, Oxid. Met. 44 (1995) 3–27.
[27] S. Hallström, M. Halvarssom, L. Höglund, T. Jonsson, J. Agren, Solid State Ionics 240 (2013) 41–50.